Materials Research Express

PAPER

Synthesis of mesoporous orthorhombic $LiMnO_2$ cathode materials via a one-step flux method for high performance lithium-ion batteries

To cite this article: Wenming Tong *et al* 2018 *Mater. Res. Express* **5** 065511

Materials Research Express

PAPER

Synthesis of mesoporous orthorhombic $LiMnO_2$ cathode materials via a one-step flux method for high performance lithium-ion batteries

RECEIVED
24 April 2018

REVISED
24 May 2018

ACCEPTED FOR PUBLICATION
1 June 2018

PUBLISHED
15 June 2018

Wenming Tong[1], **Qingxin Chu**[2,4], **Yujia Meng**[1], **Xiaofeng Wang**[1], **Bin Yang**[3], **Juanjuan Gao**[1], **Xudong Zhao**[1] **and Xiaoyang Liu**[1,4]

[1] State key Laboratory of Inorganic Synthesis and Preparative Chemistry, College of Chemistry, Jilin University, Changchun 130012, People's Republic of China
[2] College of Sciences, Shenyang Agricultural University, Shenyang 110161, People's Republic of China
[3] Center for High Pressure Science and Technology Advanced Research, Changchun 130012, People's Republic of China
[4] Author to whom any correspondence should be addressed.

E-mail: chuqx@syau.edu.cn **and** liuxy@jlu.edu.cn

Keywords: mesoporous materials, orthorhombic $LiMnO_2$, flux method, lithium ion battery

Abstract

Mesoporous orthorhombic $LiMnO_2$ has been directly fabricated by a one-step flux method in this work. Benefiting from the unique mesoporous structure, the orthorhombic $LiMnO_2$ prepared through calcinating the mixture of flux $LiOH \cdot H_2O$ and Mn_2O_3 with various Li/Mn molar ratios shows enhanced lithium storage properties. When used as the cathode for lithium ion battery, the mesoporous orthorhombic $LiMnO_2$ has been found to exhibit a maximum discharge capacity of 191.5 mAh g^{-1} and a high reversible capacity of 162.6 mAh g^{-1} (84.9% retention) after 50 cycles at a current density of 0.1 C rate. These results demonstrate its potential application in high performance lithium-ion batteries.

1. Introduction

Lithium ion batteries (LIBs) have been extensively investigated as one of the most potential electric energy storage devices because of their stable cycling lifespan, high energy density and environmental friendliness. They are promising power sources for portable electronic devices such as digital cameras, laptop computers, mobile phones, electric vehicles (EVs) and hybrid electric vehicles (HEVs) [1–4]. However, the performance improvement of LIBs still remains a challenge, which critically depends on the electrode materials [5]. Hence, it is urgently needed for the research and development of advanced electrode materials to meet the ever-increasing demands of the sustainable power sources in the modern electronics industry [6–9]. Among various electrode materials, novel carbon-based materials/composites including activated carbon aerogels [10], hierarchical porous carbon [11] and graphene@Fe_3O_4 dots/amorphous carbon [12], have been proposed as potential anode materials to substitute traditional commercial graphite because of their higher specific surface area, superior specific capacity, good electrical conductivity and excellent electrochemical stability. As the cathode for LIBs, the traditional and commercial $LiCoO_2$ cannot fulfill the requirement of high power applications such as HEVs and EVs in view of its limited specific capacity and poor capacity retention upon long cycling. As a result, other cathodes such as $LiNi_{0.5}Mn_{1.5}O_4$ [13], $LiNi_{0.76}Mn_{0.14}Co_{0.10}O_2$ [14], $LiMnO_2$ [15] and $LiVPO_4F/C$ [16], have been widely explored. Among them, $LiMnO_2$ is one of the most prospective candidates for its considerable advantages such as abundant Mn resources, intrinsic low cost, superior structural stability and environmental friendliness characteristics [17]. The theoretical discharge capacity of $LiMnO_2$ (285 mAh g^{-1}) is practically twice higher than that of spinel $LiMn_2O_4$ (148 mAh g^{-1}) [18]. Usually, layered $LiMnO_2$ has two crystal structures: orthorhombic structure and monoclinic structure [19]. The monoclinic $LiMnO_2$ is less thermodynamically stable than the orthorhombic $LiMnO_2$ and is hard to obtain as well [20]. Therefore, orthorhombic $LiMnO_2$ has been intensively studied as the potential cathode material for LIBs.

Unfortunately, orthorhombic $LiMnO_2$ still suffers from huge volume expansion and structural strain during the charge-discharge process, resulting in a rapid decrease of specific capacity and poor cycling stability, which

hampers its application in the high-energy storage system. As is well-known, the electrochemical performance of electrode materials is closely related to the morphology and structure. As a result, $LiMnO_2$ with various nanostructures and microstructures, such as microcubes [21], nanoplates [22], nanorods [23], porous microspheres [24] has been extensively explored to improve the capacity retention and rate performance for high-power LIBs. In particular, the three-dimensional (3D) porous structures are more attractive, which is attributed to the fact that their structural integrity that not only can allow a better penetration of electrolyte but also buffer the dramatic volume changes [25] during charge-discharge process, bringing in much better electrochemical performance. For example, Lv and his co-workers [26] reported that $LiMnO_2$ porous microspheres with the pore size of 200–500 nm synthesized by a molten immersion method showed a high reversible capacity of 163 mAh g^{-1} at a current density of 30 mA g^{-1} after 30 cycles and superior cyclic retention rate. Fan *et al* [24] fabricated porous spherical orthorhombic $LiMnO_2$ via a carbonate co-precipitation method, which delivered a maximum discharge capacity of 152 mAh g^{-1} at the 15th cycle and good cycling stability. Lu *et al* [27] also reported that the $LiMn_2O_4$ porous microparticles synthesized using a precipitation method followed by a high temperature calcination exhibited a high coulombic efficiency and an excellent rate capability. However, these approaches above generally involve complicated multi-step procedures, consuming long time and much energy. Hence, an advisable and scalable strategy to synthesize mesoporous orthorhombic $LiMnO_2$ with outstanding electrochemical performance is highly desired.

Herein, we report a facile one-step synthesis of mesoporous orthorhombic $LiMnO_2$ via a flux method. As the cathode of LIBs, the mesoporous orthorhombic $LiMnO_2$ can reach a maximum discharge capacity of 191.5 mAh g^{-1} at a current density of 0.1 C, superior rate capability and good cycling stability. Such significantly improved lithium storage properties may be rooted in the unique mesoporous structure, which can remarkably facilitate the electrolyte infiltration and Li^+ intercalation and easily accommodate to the volume changes during the reversible electrochemical process.

2. Experimental

2.1. Preparation of mesoporous orthorhombic $LiMnO_2$ cathode materials

Materials and reagents were of analytical grade and directly used as received without further purification. The synthesis of mesoporous orthorhombic $LiMnO_2$ was carried out by a one-step flux method using $LiOH \cdot H_2O$ and Mn_2O_3 as starting materials. In a typical synthesis, 15.75 mmol $LiOH \cdot H_2O$ and 7.5 mmol Mn_2O_3 with Li/Mn molar ratio of 1.05, were grounded homogeneously for 30 min in an agate mortar. Then the well-mixed powders were put into a tube furnace and calcined at 600 °C for 3 h under vacuum. After cooling down to room temperature, the product was washed with distilled water and then was dried at 60 °C in a oven overnight. The as-prepared sample was labeled as LMO-1. For comparison, LMO-2 sample was prepared with the same process mentioned as above except using 25 mmol $LiOH \cdot H_2O$ and 5 mmol Mn_2O_3 with Li/Mn molar ratio of 2.50. Moreover, LMO-3 sample was prepared with the same process mentioned as above except using 30 mmol $LiOH \cdot H_2O$ and 3 mmol Mn_2O_3 with Li/Mn molar ratio of 5.00.

2.2. Material characterizations

Powder x-ray diffraction (XRD) patterns were obtained from a Rigaku D/MAX 2550 diffractometer with Cu Kα radiation ($\lambda = 1.5418$ Å). Scanning electron microscopy (SEM) images were taken with a JEOL JSM-6700F microscope operating at 5 kV. Transmission electron microscopy (TEM) analysis and high resolution transmission electron microscopy (HRTEM) analysis were performed on a FEI Tecnai G2 F20 s-twin D573 transmission electron microscope with an acceleration voltage of 200 kV. The nitrogen adsorption-desorption measurements were carried out with a Micromeritics ASAP 2420 surface area analyzer by using Brunauer–Emmett–Teller (BET) method at 77 K. Pore size distribution plots were obtained from the desorption branch of the isotherms using the Barrett–Joyner–Halenda (BJH) model.

2.3. Electrochemical measurements

The electrochemical characteristics of the samples were evaluated using CR2025 coin cells. The working electrode was prepared by mixing the slurry of obtained orthorhombic $LiMnO_2$ active material, acetylene black and polyvinylidene fluoride (PVDF) binder with a weight ratio of 8:1:1 in N-methyl-2-pyrrolidone (NMP) solvent. After stirring for 5 h, the slurry was coated onto an aluminum foil substrate and dried at 120 °C for 13 h in a vacuum oven, followed by cutting into small disks as cathodes. The mass loading of the active material on the electrode was 1–2 mg cm^{-2}. Lithium metal was used as the counter electrode and Celgard 2400 microporous membrane was used as the separator. The electrolyte was 1 M $LiPF_6$ in EC/DEC (1:1 v/v). All CR2025 coin-type cells were assembled in an argon-filled glove box. The galvanostatic charge-discharge measurements were

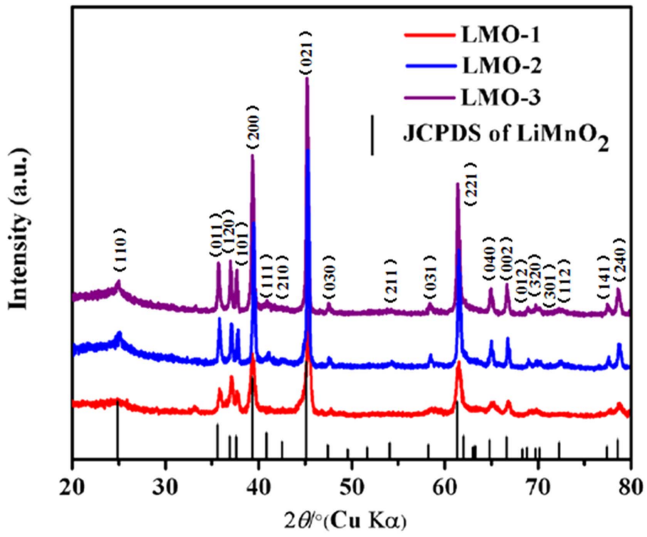

Figure 1. XRD patterns of the orthorhombic $LiMnO_2$ samples: LMO-1, LMO-2 and LMO-3.

carried out at room temperature with various current densities in the voltage range of 2.0–4.4 V by the LAND battery testing system (CT2001A).

3. Results and discussion

Figure 1 displays the XRD patterns of the as-synthesized $LiMnO_2$ samples. It can be seen that all the diffraction peaks can be basically indexed to the orthorhombic $LiMnO_2$ with a space group of *Pmnm*, which corresponds to JCPDS No. 35-0749.

Moreover, it can be found that the diffraction peaks become more intense with the increase of Li/Mn molar ratios from 1.05 to 5.00, especially for the (110) peak, demonstrating higher crystallinity. The broader and weaker (110) peak can be observed for LMO-1 sample, which may be related to its smaller crystalline size and higher degree of disorder [28]. Furthermore, the higher full-width-at-half-maximum (FWHM) value of the (110) peak indicates that there are more stacking faults between Mn and Li sites [29], which directly affects the electrochemical characteristics. According to the literatures, the orthorhombic $LiMnO_2$ with a weak crystallinity, more stacking faults and smaller crystallites tends to exhibit a higher discharge capacity [30].

The morphology and structure of the orthorhombic $LiMnO_2$ samples have been further examined by SEM and TEM analyses. As shown in figure 2, the as-synthesized orthorhombic $LiMnO_2$ samples are assembled by closely packed primary nanocrystallites with irregularly shaped pores among them. The size of the primary nanocrystallites is approximately 20–30 nm in diameter. The average size of the aggregated primary nanocrystallites slightly becomes larger when the Li/Mn molar ratios increase from 1.05 to 5.00, as displayed in figures 2(a)–(c). This may be ascribed to the fact that the increase of the Li/Mn molar ratio dramatically accelerates the process of dissolution and recrystallization, leading to the formation of the larger crystallites [31]. To further demonstrate their detailed structures, the obtained orthorhombic $LiMnO_2$ samples were characterized by TEM. Figure 2(d) depicts the low magnification TEM image of LMO-1 sample. Notably, the obtained LMO-1 sample is consisted of aggregated primary nanoparticles of approximately 30 nm in diameter and their extremely rough surfaces are connected together to create a high inter-particle porosity. The representative high-resolution TEM image of the primary nanoparticles observed from the figure 2(d) inset indicates that the lattice fringe of the sample is 0.36 nm, corresponding to the (110) plane of the orthorhombic $LiMnO_2$. This result is in accordance with the XRD analysis.

The porous characteristics and specific surface areas of the as-synthesized $LiMnO_2$ samples were further explored by nitrogen adsorption-desorption measurements. Figures 3(a), (b) show the nitrogen adsorption-desorption isotherms and corresponding pore size distributions of the orthorhombic $LiMnO_2$ samples. It can be seen that the LMO-1 sample has a typical hysteresis loop and its N_2 adsorption quantity is much higher than that of other samples, as observed in figure 3(a), suggesting its abundant mesoporous structure. The BET specific surface areas of the LMO-1, LMO-2 and LMO-3 sample are 3.99 $m^2 g^{-1}$, 2.25 $m^2 g^{-1}$ and 1.82 $m^2 g^{-1}$, respectively. Figure 3(b) further confirms that the typical pore size of the LMO-1 sample is around 45 nm, which is in good agreement with the SEM and TEM analyses. The improved specific surface area and unique

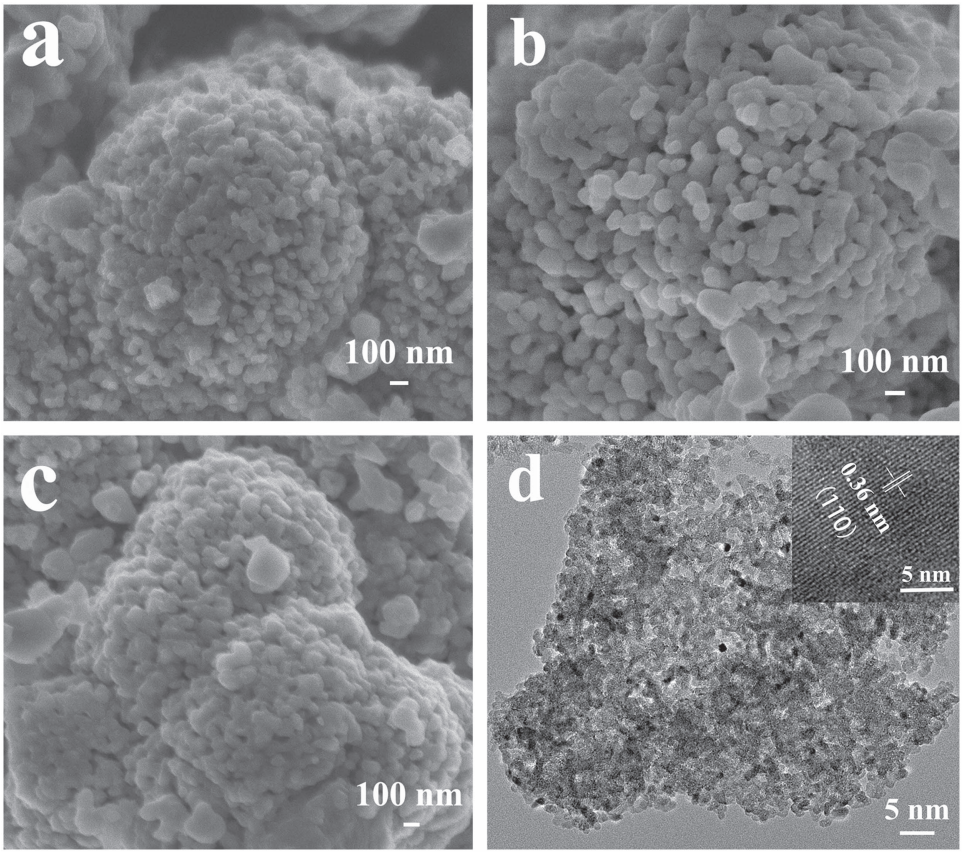

Figure 2. SEM and TEM images of the orthorhombic $LiMnO_2$ samples: (a), (d) LMO-1; (b) LMO-2; (c) LMO-3.

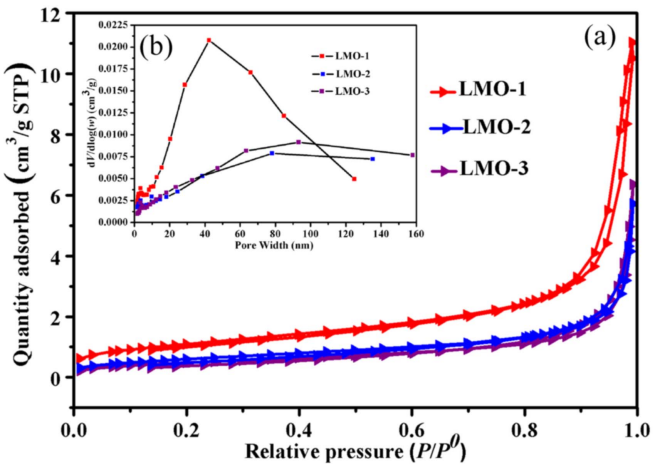

Figure 3. (a) N_2 adsorption-desorption isotherms and (b) corresponding pore size distributions of the orthorhombic $LiMnO_2$ samples: LMO-1, LMO-2 and LMO-3.

mesoporous structure of the LMO-1 sample may be more desirable for lithium storage properties, which may be attributed to the fact that the improved specific surface area may allow better contact area between electrode and electrolyte, fast Li^+ diffusion as well as reduced charge-transfer resistance. Moreover, the hierarchical porous structure can act as a buffer layer to alleviate the volume expansion of the electrode during the lithiation/delithiation process.

The electrochemical performance of the $LiMnO_2$ samples for LIBs was further performed by the galvanostatic charge-discharge measurements. Figures 4(a), (b) present the charge-discharge profiles and cyclic performance of the orthorhombic $LiMnO_2$ samples. Cycling stability tests were carried out at a current density of 0.5 C in the voltage range of 2.0–4.4 V. As shown in figure 4(a), all of the orthorhombic $LiMnO_2$ samples

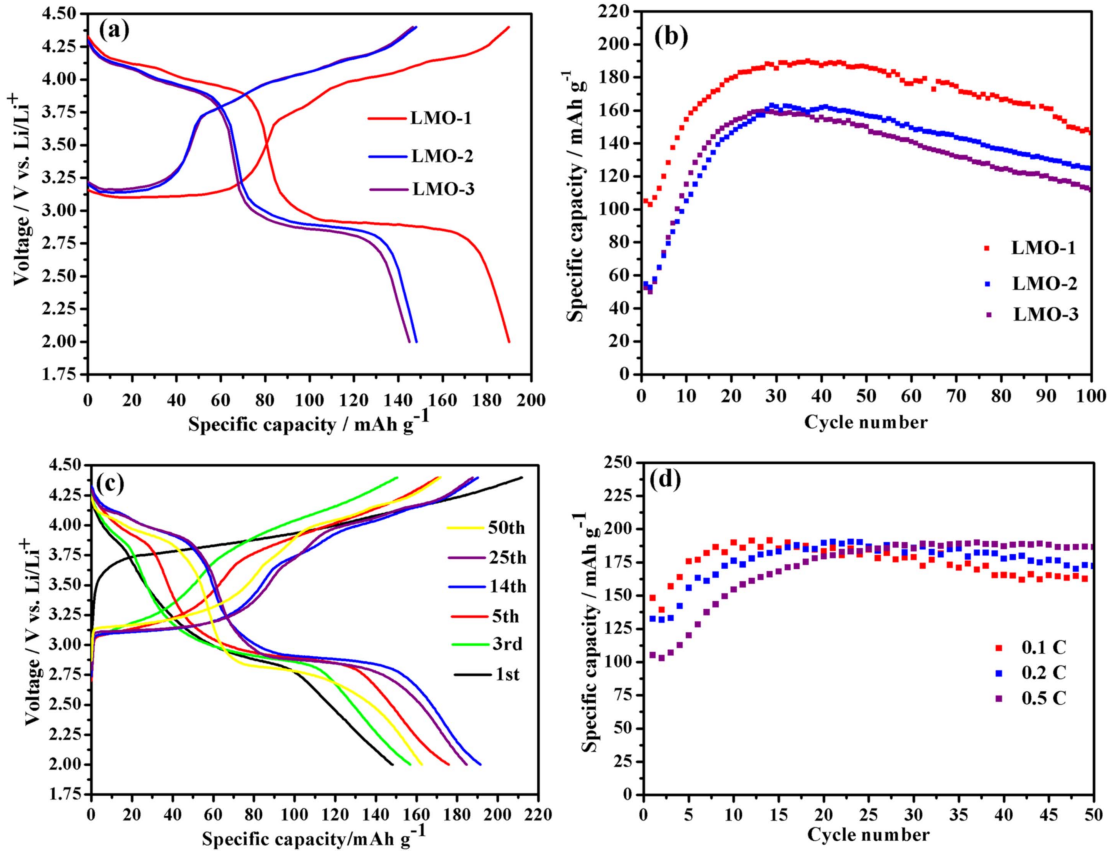

Figure 4. (a) The charge-discharge curves of the cycle with the maximum discharge capacity and (b) cyclic performance of the orthorhombic $LiMnO_2$ samples: LMO-1, LMO-2 and LMO-3. Cycling was carried out at a current density of 0.5 C in the voltage range of 2.0–4.4 V. (c) The typical charge-discharge curves and (d) cyclic performance of the LMO-1 sample. Cycling was carried out at current densities of 0.1 C, 0.2 C and 0.5 C in the voltage range of 2.0–4.4 V.

display two distinct voltage plateaus at around 4 V and 3 V, which may be a result of phase transition during the cycling from orthorhombic $LiMnO_2$ to spinel phase. The different plateaus represent that Li^+ intercalates on different sites: tetrahedral site and octahedral site in the cycle-induced spinel $LiMn_2O_4$ [32]. From the charge and discharge profiles, it can be seen that the maximum discharge capacities of LMO-1, LMO-2 and LMO-3 sample are 190.0 mAh g^{-1}, 148.3 mAh g^{-1} and 145.0 mAh g^{-1}, respectively. Clearly, the LMO-1 sample shows enhanced specific capacity, which may be ascribed to its unique small size and interconnected porous network architectures. As reported previously [33], the capacity loss of the orthorhombic $LiMnO_2$ materials was mainly due to the decrease of the length in the 3 V plateau, which might be predominantly caused by the collective Jahn-Teller distortion of the cycle-induced spinel phase [34]. Additionally, the dissolution of manganese could directly lead to defective spinels [35] and poor cycling performance. However, the charge-discharge curves of the LMO-1 sample show a longer and more flat 3 V plateau compared with those of other samples, which indicates that it is more stable and can better accommodate the volume changes resulting from the phase transformation during the charge-discharge process. The cycling stability of the orthorhombic $LiMnO_2$ samples was further investigated as the cathode for LIBs. As shown in figure 4(b), the reversible capacities of the LMO-1, LMO-2 and LMO-3 sample can be sustained at 146.3 mAh g^{-1}, 113.4 mAh g^{-1} and 101.6 mAh g^{-1} at a current density of 0.5 C after 100 cycles, corresponding with the retention rates of 77.0%, 76.5% and 70.1%, respectively. Figure 4(c) is the characteristic charge-discharge curves of the LMO-1 sample. The initial charge and discharge capacities of the LMO-1 sample are about 211.9 mAh g^{-1} and 148.2 mAh g^{-1} at a current density of 0.1 C, corresponding to the coulombic efficiency of 69.9%. As reported by Shu *et al* [36], the large irreversible capacity was attributed to the phase transition from the orthorhombic $LiMnO_2$ to spinel $LiMn_2O_4$. Moreover, a slowly increase in the length of the plateau at 3 V and 4 V with further cycling has been observed, suggesting that both the spinel-like phase and the Li^+ intercalation on tetrahedral sites have developed further. The discharge capacity of the LMO-1 sample can gradually reach the maximum value of 191.5 mAh g^{-1} at the 14th cycle, of which the 3 V plateau representing Li intercalation on octahedral sites becomes the longest among all discharge cycles. The initial discharge capacity is lower than the maximum value at the first few cycles, which is attributed to the enhancement of Li^+ diffusivity in the host by the activation process [37]. After 50 cycles, the charge and

discharge capacities can be maintained at 171.8 mAh g^{-1} and 162.6 mAh g^{-1}, corresponding to the coulombic efficiency of 94.6%. To further investigate the application of the product in high power density devices, the rate cycling test of the LMO-1 sample was performed at current densities of 0.1 C, 0.2 C and 0.5 C in the voltage range of 2.0–4.4 V. As displayed in figure 4(d), the initial discharge capacities of the LMO-1 sample are 148.2, 132.6 and 105.2 mAh g^{-1} at current densities of 0.1 C, 0.2 C and 0.5 C, respectively. Then the discharge capacities gradually reach the maximum values of 191.5, 190.6 and 190.0 mAh g^{-1} at the 14th, 21th and 37th cycle, respectively. After 50 cycles, the discharge capacities of the LMO-1 sample still can be maintained at 162.6, 172.3 and 186.5 mAh g^{-1} at current densities of 0.1 C, 0.2 C and 0.5 C, suggesting its good cycling stability. It is noteworthy that when the current density is 0.5 C, the LMO-1 sample shows a lower initial capacity, longer activation time and much better cycling durability than that of 0.1 C and 0.2 C after 50 cycles. This can be ascribed to the fact that the LMO-1 sample may suffer from a ultrafast and incomplete charge-discharge process at a high rate and some residual lithium ions in the electrode materials have no sufficient time to finish the more complete intercalation and extraction process [38]. These results above reveal that the LMO-1 sample can be regard as an excellent cathode material for LIBs.

4. Conclusions

In summary, mesoporous orthorhombic $LiMnO_2$ has been successfully fabricated by a one-step flux method. After a series of thorough tests, such mesoporous orthorhombic $LiMnO_2$ can deliver a initial discharge capacity of 148.2 mAh g^{-1} at a current density of 0.1 C. Then the specific capacity gradually increases to a maximum value of 191.5 mAh g^{-1} in the first few cycles, which may be attributed to the activation process of electrode materials. After 50 cycles, a high specific capacity of 162.6 mAh g^{-1} can be still achieved. The abundant mesoporous structure, improved specific surface area and optimal primary nanoparticle size of the orthorhombic $LiMnO_2$ may be responsible for the superior lithium storage properties and good cycling stability. Notably, the successful fabrication of mesoporous orthorhombic $LiMnO_2$ not only can offer a promising cathode material for advanced LIBs, but also will inspire the fabrication of high performance electrode materials for electrochemical energy storage applications.

Acknowledgments

We would like to gratefully acknowledge the support from the National Natural Science Foundation of China (Grants 21271082 and 21601127).

ORCID iDs

Xiaoyang Liu https://orcid.org/0000-0002-7128-8457

References

[1] Gao Z, Sun H, Fu L, Ye F, Zhang Y, Luo W and Huang Y 2018 Promises, challenges, and recent progress of inorganic solid-state electrolytes for all-solid-state lithium batteries *Adv. Mater.* **30** 1705702
[2] Hannan M A, Lipu M S H, Hussain A and Mohamed A 2017 A review of lithium-ion battery state of charge estimation and management system in electric vehicle applications: challenges and recommendations *Renewable Sustainable Energy Rev.* **78** 834–54
[3] Park K J, Choi M J, Maglia F, Kim S J, Kim K H, Yoon Chong S and Sun Y K 2018 High-capacity concentration gradient $Li[Ni_{0.865}Co_{0.120}Al_{0.015}]O_2$ cathode for lithium-ion batteries *Adv. Energy Mater.* **0** 1703612
[4] Ariyoshi K, Yamamoto H and Yamada Y 2018 High dimensional stability of $LiCoMnO_4$ as positive electrodes operating at high voltage for lithium-ion batteries with a long cycle life *Electrochim. Acta* **260** 498–503
[5] Ullah A, Majid A and Rani N 2018 A review on first principles based studies for improvement of cathode material of lithium ion batteries *J. Energy Chem.* **27** 219–37
[6] Sun Y, Cong H, Zan L and Zhang Y 2017 Oxygen vacancies and stacking faults introduced by low-temperature reduction improve the electrochemical properties of Li_2MnO_3 nanobelts as lithium-ion battery cathodes *ACS Appl. Mater. Interfaces* **9** 38545–55
[7] Liao L, Wang H, Guo H, Zhu P, Xie J, Jin C, Zhang S, Cao G, Zhu T and Zhao X 2015 Facile solvothermal synthesis of ultrathin $LiFe_xMn_{1-x}PO_4$ nanoplates as advanced cathodes with long cycle life and superior rate capability *J. Mater. Chem.* A **3** 19368–75
[8] Kong D, Li X, Zhang Y, Hai X, Wang B, Qiu X, Song Q, Yang Q-H and Zhi L 2016 Encapsulating V_2O_5 into carbon nanotubes enables the synthesis of flexible high-performance lithium ion batteries *Energy Environ. Sci.* **9** 906–11
[9] Guo J, Cai Y, Zhang S, Chen S and Zhang F 2016 Core–shell structured o-$LiMnO_2$@Li_2CO_3 nanosheet array cathode for high-performance, wide-temperature-tolerance lithium-ion batteries *ACS Appl. Mater. Interfaces* **8** 16116–24
[10] Yang X, Wei C and Zhang G 2016 Activated carbon aerogels with developed mesoporosity as high-rate anodes in lithium-ion batteries *J. Mater. Sci.* **51** 5565–71
[11] Yang X, Wei C, Sun C, Li X and Chen Y 2017 High performance anode of lithium-ion batteries derived from an advanced carbonaceous porous network *J. Alloys Compd.* **693** 777–81

[12] Li C, Li Z, Ye X, Yang X, Zhang G and Li Z 2018 Crosslinking-induced spontaneous growth: a novel strategy for synthesizing sandwich-type graphene@Fe_3O_4 dots/amorphous carbon with high lithium storage performance *Chem. Eng. J.* **334** 1614–20
[13] Yin C, Zhou H, Yang Z and Li J 2018 Synthesis and electrochemical properties of $LiNi_{0.5}Mn_{1.5}O_4$ for li-ion batteries by the metal-organic framework method *ACS Appl. Mater. Interfaces* **10** 13625–34
[14] Zheng J, Yan P, Estevez L, Wang C and Zhang J-G 2018 Effect of calcination temperature on the electrochemical properties of nickel-rich $LiNi_{0.76}Mn_{0.14}Co_{0.10}O_2$ cathodes for lithium-ion batteries *Nano Energy* **49** 538–48
[15] Yang D, Zhao H, Wang J, Sun Y, Wu N and Tian W 2014 Effects of constant voltage at low potential on the formation of $LiMnO_2$/graphite lithium ion battery *J. Solid State Electrochem.* **18** 1907–14
[16] Xiong Z, Zhang G, Xiong J, Yang X and Zhang Y 2013 Modified sol–gel synthesis of nanosized $LiVPO_4F$/C cathode material with mechanical blending assist *Mater. Lett.* **111** 214–6
[17] Ji H, Miao X, Wang L, Qian B and Yang G 2014 Effects of microwave-hydrothermal conditions on the purity and electrochemical performance of orthorhombic $LiMnO_2$ *ACS Sustainable Chem. Eng.* **2** 359–66
[18] Yang F, Zhang Q, Hu X, Peng T and Liu J 2017 Preparation of Li-rich layered-layered type $xLi_2MnO_3\cdot(1-x)LiMnO_2$ nanorods and its electrochemical performance as cathode material for Li-ion battery *J. Power Sources* **353** 323–32
[19] Li X, Su Z and Wang Y 2018 Electrochemical properties of monoclinic and orthorhombic $LiMnO_2$ synthesized by a one-step hydrothermal method *J. Alloys Compd.* **735** 2182–9
[20] Zhou H, Li Y, Zhang J, Kang W and Yu D Y W 2016 Low-temperature direct synthesis of layered m-$LiMnO_2$ for lithium-ion battery applications *J. Alloys Compd.* **659** 248–54
[21] Xu H, Sun J and Gao L 2013 Hydrothermal synthesis of $LiMnO_2$ microcubes for lithium ion battery application *Ionics* **19** 63–9
[22] He Y, Li R, Ding X, Jiang L and Wei M 2010 Hydrothermal synthesis and electrochemical properties of orthorhombic $LiMnO_2$ nanoplates *J. Alloys Compd.* **492** 601–4
[23] Xiao X, Wang L, Wang D, He X, Peng Q and Li Y 2009 Hydrothermal synthesis of orthorhombic $LiMnO_2$ nano-particles and $LiMnO_2$ nanorods and comparison of their electrochemical performances *Nano Res.* **2** 923–30
[24] Fan G, Zeng Y, Chen R and Lü G 2008 Microstructure and electrochemical characterization of spherical-like orthorhombic $LiMnO_2$ via co-precipitation *J. Alloys Compd.* **461** 267–72
[25] Zhang H, Li Z, Yu S, Xiao Q, Lei G and Ding Y 2016 Carbon-encapsulated $LiMn_2O_4$ spheres prepared using a polymer microgel reactor for high-power lithium-ion batteries *J. Power Sources* **301** 376–85
[26] Lv Y, Mei T, Gong H, Wei D, Xing Z, Zhu Y and Qian Y 2012 Synthesis of $LiMnO_2$ porous microsphere and its electrochemical behaviour as cathode material in lithium-ion batteries *Micro Nano Lett.* **7** 439
[27] Lu J, Zhou C, Liu Z, Lee K S and Lu L 2016 $LiMn_2O_4$ cathode materials with large porous structure and radial interior channels for lithium ion batteries *Electrochim. Acta* **212** 553–60
[28] Croguennec L, Deniard P and Brec R 1997 Electrochemical cyclability of orthorhombic $LiMnO_2$: characterization of cycled materials *J. Electrochem. Soc.* **144** 3323–30
[29] Kim T-J, Son D, Cho J and Park B 2006 Enhancement of the electrochemical properties of o-$LiMnO_2$ cathodes at elevated temperature by lithium and fluorine additions *J. Power Sources* **154** 268–72
[30] Croguennec L, Deniard P, Brec R, Biensan P and Broussely M 1996 Electrochemical behavior of orthorhombic $LiMnO_2$: influence of the grain size and cationic disorder *Solid State Ion.* **89** 127–37
[31] Wang Y, Shao X, Xu H, Xie M, Deng S, Wang H, Liu J and Yan H 2013 Facile synthesis of porous $LiMn_2O_4$ spheres as cathode materials for high-power lithium ion batteries *J. Power Sources* **226** 140–8
[32] Liu Q, Mao D, Chang C and Huang F 2007 Phase conversion and morphology evolution during hydrothermal preparation of orthorhombic $LiMnO_2$ nanorods for lithium ion battery application *J. Power Sources* **173** 538–44
[33] He Y, Feng Q, Zhang S, Zou Q, Wu X and Yang X 2013 Strategy for lowering Li source dosage while keeping high reactivity in solvothermal synthesis of $LiMnO_2$ nanocrystals *ACS Sustainable Chem. Eng.* **1** 570–3
[34] Li C, Zhang H P, Fu L J, Liu H, Wu Y P, Rahm E, Holze R and Wu H Q 2006 Cathode materials modified by surface coating for lithium ion batteries *Electrochim. Acta* **51** 3872–83
[35] Chiang Y-M, Wang H and Jang Y-I 2001 Electrochemically induced cation disorder and phase transformations in lithium intercalation oxides *Chem. Mater.* **13** 53–63
[36] Shu Z X, Davidson I J, McMillan R S and Murray J J 1997 Electrochemistry of $LiMnO_2$ over an extended potential range *J. Power Sources* **68** 618–22
[37] Chen S, Cao F, Liu F, Xiang Q, Feng X, Liu L and Qiu G 2014 Facile hydrothermal synthesis and electrochemical properties of orthorhombic $LiMnO_2$ cathode materials for rechargeable lithium batteries *RSC Adv.* **4** 13693–703
[38] Zaghib K, Goodenough J B, Mauger A and Julien C 2009 Unsupported claims of ultrafast charging of $LiFePO_4$ Li-ion batteries *J. Power Sources* **194** 1021–3